minerals

MDPI

Article

Composition and Genesis of Serpentinite-Type Nephrite, Mount Bikilyar, South Urals, Russia

Evgeniy V. Kislov [1,*] and Valeriy V. Murzin [2]

[1] Dobretsov Geological Institute of the Siberian Branch of the Russian Academy of Sciences, 670047 Ulan-Ude, Russia
[2] Zavaritskiy Institute of Geology and Geochemistry of the Uralian Branch of the Russian Academy of Sciences, 620110 Ekaterinbourg, Russia; murzin@igg.uran.ru
* Correspondence: evg-kislov@ya.ru

Abstract

The object of this study is nephrite found on Mount Bikilyar, South Urals, Russia. The purpose of the study is to determine the mineral and chemical composition of the nephrite and host rocks and to develop a model of the nephrite's formation. The mineral composition was studied using a scanning electron microscope with an energy-dispersive quantitative microanalysis system. We studied the chemical, trace element, and oxygen isotopic composition. The nephrite's composition is dominated by tangled fibrous and downy aggregates, with large lamellar grains of actinolite. Magnesian hornblende and resorbed diopside grains, as well as chromite, titanite, apatite, chlorite, sulfides, and secondary minerals, are less common. The host rocks are metagabbro of diverse mineral compositions. The nephrite is characterized by a subchondritic trough-like distribution spectrum of REE with a negative Eu anomaly. The chondrite-normalized spectrum of the metagabbro is characterized by significantly higher REE content values. The $\delta^{18}O$ isotopic composition of the nephrite is +5.53 to +5.80‰, indicating the deep origins of oxygen inherited from ultramafic rocks. The extremely heterogeneous and heavier composition of the metagabbro is +4.42 to +11.27‰, reflecting different contributions of the mantle and crustal sources to its formation. The nephrite was formed as a result of ultramafic xenoblock transformation under the influence of gabbro. Initially, serpentine was replaced by diopside, after which actinolite developed to form the nephrite. The Bikilyar nephrite differs in its mineral composition from the nephrite of other deposits. Despite the unique mineral composition, Bikilyar nephrite is a typical serpentinite in terms of paragenesis and chemical composition. The nephrite-specific mineral and chemical composition is explained by the small size of the ultramafic block that is in a significant volume of gabbro.

Keywords: actinolite; diopside; rare earth elements; oxygen isotopic composition

Check for updates

Academic Editors: Guanghai Shi and Tianlong Jiang

Received: 2 July 2026
Revised: 1 August 2026
Accepted: 2 August 2026
Published: 7 August 2026

Copyright: © 2026 by the authors. Licensee MDPI, Basel, Switzerland. This article is an open access article distributed under the terms and conditions of the Creative Commons Attribution (CC BY) license.

1. Introduction

Nephrite is a fibrous, cryptocrystalline rock composed of minerals of the tremolite–ferroactinite series, primarily tremolite. Nephrite is a highly sought-after gemstone in the jewelry and ornamental sectors, used since ancient times for the production of tools, jewelry and religious objects. Its use is particularly popular in China, New Zealand, and on the Pacific coast of North America [1–5].

According to its origin and composition, there are two endogenous types of nephrite [1,6]. The first type is nephrite related to serpentinite ophiolites, while the second type is related

to dolomite in tremolite–calcite magnesian skarns. The exogenous geological–industrial type is represented by placers; alluvial placers are the most productive. The color of the serpentinite-type (S-type) nephrite is characterized by various shades of green, and less often brown and black, while the dolomite-type nephrite color is characterized by a wide range of predominantly light shades, from white and gray to light green, and less often brown and black. The most prized nephrite colors are bright bluish-green with a minimal number of chromite grains, white, and iridescent cat's eye. Alluvial pebbles are highly prized, especially those with red, brown, or black surface edges [7].

Unlike in China, the majority of nephrite deposits in Russia are of the S type, which will be discussed further. The State Balance of Mineral Reserves of Russia includes 28 nephrite deposits; 20 of them are S-type (Figure 1). The following deposits of S-type nephrite were mined in 2024: Ospa and Sagan-Sair in the Oka district, Khamarkhuda in the Zakamensk district of Buryatia, and Kantegir in Krasnoyarsk Krai [8].

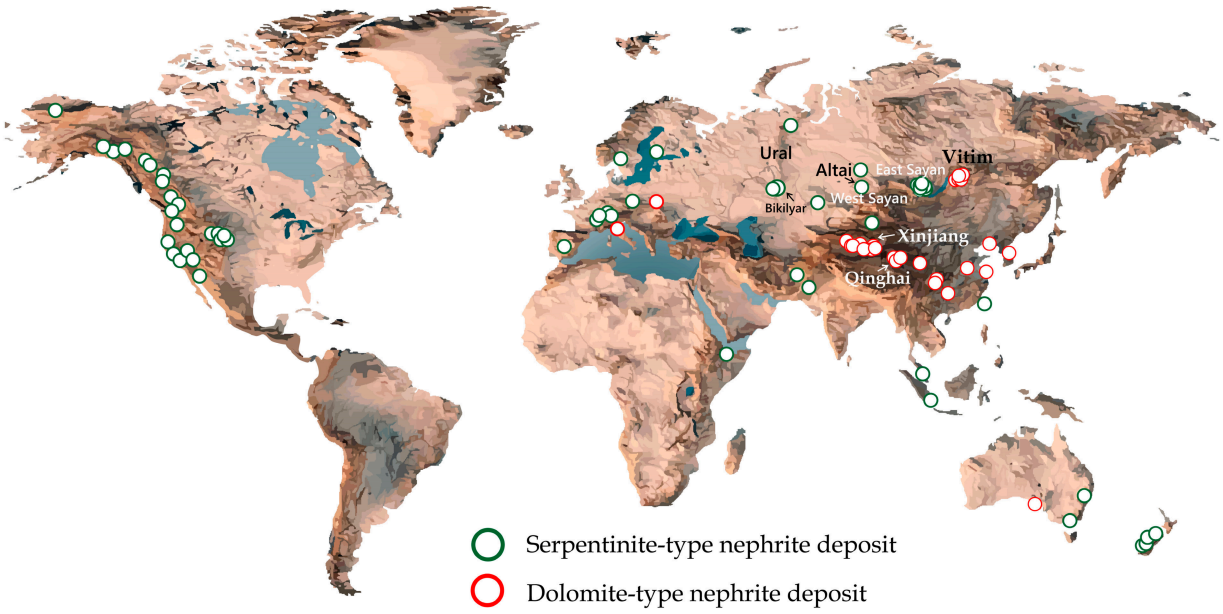


Figure 1. Nephrite deposits around the world.

The Eastern Sayan nephrite province is located within the Oka district of Buryatia and the Nizhneudinsk and Cheremkhovo districts of the Irkutsk region. The Dzhida nephrite province is located on the Khamar–Daban ridge within the Zakamensk and Tunka districts of Buryatia. The Western Sayan province is located in the Ermakovo and Shushensk districts of the Krasnoyarsk Krai, Piy-Khem, Tes-Khem and Kaa-Khem districts of Tyva [3]. Param is the only S-type nephrite deposit in the Vitim nephrite province of the Muya district of Buryatia [3]. The Altai nephrite province is located in the Mayma, Turochak and Ust-Koksa districts of the Altai Republic [9–11]. A number of occurrences are located outside above-mentioned provinces: Munilkan (Selenyakh) in the Mom district of Yakutia [12], Kuyul in the Penzhin district of Kamchatka [13], and Malo-Kyafar in the Zelenchuk district of the Karachay-Cherkess Republic [14–16].

The Ural province is known for finds near Muldakaevo in the Beloretsk district of Bashkiria [17] and on Mount Bikilyar near Miass town [18]. There is a Nyrdvomenshor deposit in the Polar Urals [19,20]. In the Middle Urals, nephrite was found on Mount Listvennaya near the Pyshma [21] and the Bazhenov chrysotile–asbestos deposit [22]. There is an Akademicheskoe deposit near Miass [23,24]. Three occurrences of nephrite were found in Bashkiria: Kozma-Demyan in the northeast, Keushtin in the southeast, and Kildigul in the southwest [25]. There is the Khalilov deposit in the Orenburg region and

the Dzhetygara (Zhitikara) occurrence in the Kostanay region of Kazakhstan in the South Urals [3].

There are few deposits of S-type nephrite outside Russia. Deposits of dolomite type nephrite predominate in China [26] (Figure 1). The S-type nephrite deposits are located in Xinjiang [27–31], Qinghai [32,33], Sichuan [34], and Taiwan [35–38]. Nephrite from the borders of Pakistan [39–43] and Afghanistan [44,45] has recently been found. Occurrences in the Shaitantas in the Karaganda region of Kazakhstan [3], Ko Phuong in the Son La province of Vietnam [46], and areas of Papua New Guinea [47] are insufficiently studied. A number of deposits are located on the Pacific coast of North America, and the exploration is carried out mainly in British Columbia in Canada [48–51], and, to a lesser extent, in USA—Washington [52–54] and California [55]. Deposits have long been acknowledged in Wyoming, USA [56–61]. In Europe, finds of nephrite are rare, although they have long been acknowledged. The Jordanow and Naslawice deposits in Poland were mined in the 19th century [60,62,63]. Nephrite has been observed in the Alps, Apennines, Harz, and Scandinavia. It is particularly abundant in the canton of Graubünden (Grisons) in Switzerland. There is a well-known occurrence in Schwarzenbach-an-der-Saale in the Franconian Forest, Bavaria, Germany. There is nephrite in the moraine deposits of Scandinavian origin. Nephrite pebbles and boulders, "Mur nockerls", have been found in the alluvium of the Mur River between Leoben and Graz in Austria [2]. Small deposits have long been acknowledges on the South Island of New Zealand [5,60,64–69] and in the province of New South Wales in Australia [70,71].

According to most researchers, S-type nephrite is metasomatically formed upon contact between serpentinites and gabbro or granite metasomatites [1,3,6,23,52,60], as well as metamorphic rocks of aluminosilicate composition [6,23,26,50,51]. Formation of nephrite inside the bodies of ultramafic rocks [23], mafic metamorphosed rocks [3,61], and gabbro or granite metasomatites [3] is less frequently indicated. Other researchers insist on the metamorphic formation of nephrite in the zones of serpentinite mélange [26,72].

Recent studies of the Urals' deposits of S-type nephrite show how diverse its origin can be: in the quarry of the Bazhenov deposit, nephrite formation in serpentinite upon contact with intrusive bodies is clearly visible [22], and the Nyrdvomenshor deposit is confined to the zone of serpentinite mélange in the Main Ural Fault zone [20]. The nephrite occurrence at Mount Bikilyar is different. Therefore, the purpose of this study is to determine the Mount Bikilyar nephrite localization and composition features. The goal is to formulate a model for its formation based on these features.

2. Materials and Methods

Six samples were taken from bedrock outcrops at the top of Mount Bolshoi (Big) Bikilyar (Figure 2). Two samples of nephrite, B1 and B1/1; nephrite with inclusions of diopside, B2 (Figure 3); green metagabbro with magnetite crystals, B3; dark-colored metagabbro, B4; and light-colored metagabbro, B5 (Figure 4) were studied. Visual petrographic and mineralogical studies were carried out under natural light using photographic recording.

Mineral composition was studied using an LEO-1430VP scanning electron microscope (Carl Zeiss, Oberkochen, Baden-Württemberg, Germany) with an INCA Energy 350 energy-dispersive microanalysis system (Oxford Instruments, High Wycombe, Buckinghamshire, UK) at the "Geospektr" Center (GIN SB RAS, Ulan-Ude). The study conditions were as follows: accelerating voltage 20 kV, probe current 0.3–0.4 nA, probe size < 0.1 microns, measurement time 50 s, and analysis error of 2–4 rel. % depending on the surface quality of the sample and the characteristics of its composition. An interactive software package, Incapture Exreport ver. 3.14.06, developed at GIN SB RAS, was used to process the research results. The program implements an original method for identifying mineral phases based

on mineral stoichiometry. The program's output is a report in the form of Excel tables containing data on concentrations of elements and components, atomic percentages, and formulas calculated taking into account the identification of minerals. For a number of minerals (chromite, epidote, garnet, magnetite, muscovite, pyroxene, spinel, ilmenite), the content of divalent and trivalent iron is calculated by iterative fitting to stoichiometry using the golden ratio. The full results are shown in the Supplementary Files.

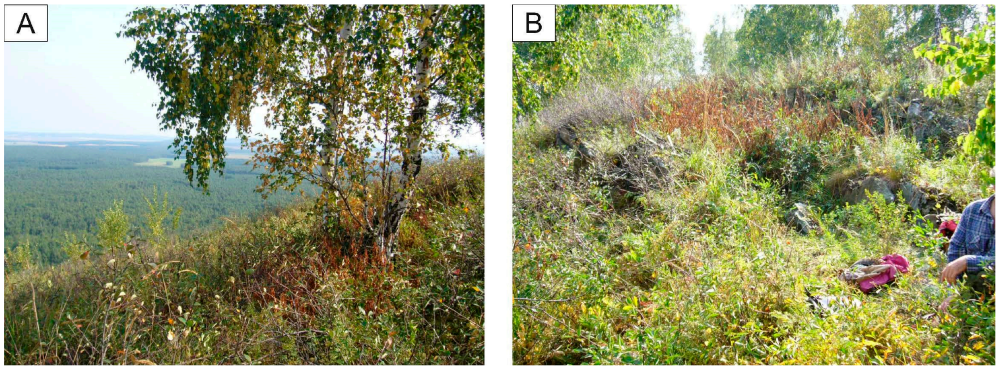


Figure 2. Mount Bolshoy (Big) Bikilyar: (**A**)—View from the nephrite outcrop to the east; (**B**)—Outcrops.

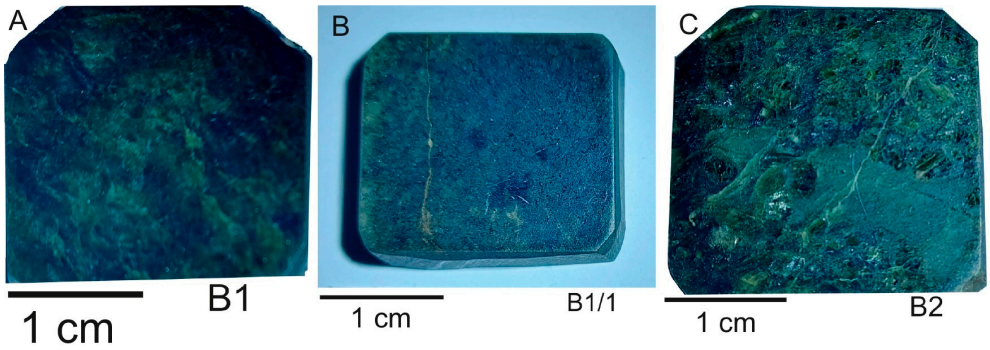


Figure 3. Polished sections of nephrite of heterogeneous color, with inclusions of diopside (B2) and fracturing: (**A**)—B1, (**B**)—B1/1, (**C**)—B2.

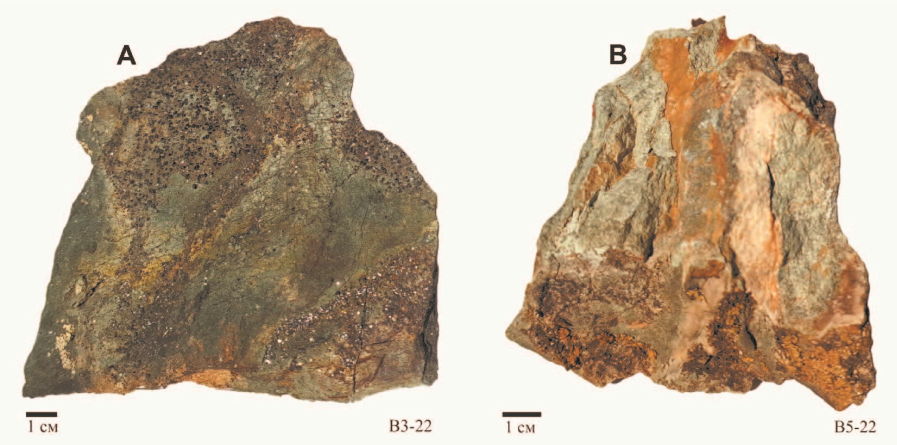


Figure 4. Samples of metagabbro: (**A**)—B3, (**B**)—B5.

Macro component analysis was carried out at the "Geospektr" Center (GIN SB RAS, Ulan-Ude): SiO_2, TiO_2, Al_2O_3, and P_2O_5 were determined by the photometric method; CaO, MgO, MnO, Fe_2O_3, and CO_2 by atomic absorption spectroscopic method; FeO and CO_2 by the titrimetric method; LPP and S by gravimetric method; Na_2O and K_2O by the

flame photometric method; and Cr, V, Co, Ni, and Cu by the atomic emission spectral method. The samples were analyzed twice, in different parts of the samples.

Trace element content was determined at the "Geoanalytik" Center (IGG UB RAS) using a NexION300S quadrupole ICP mass spectrometer (Perkin Elmer, Shelton, Connecticut, USA). Microwave digestion of the samples was carried out with a mixture of acids HCl + HNO_3 + HF using a Berghof Speedwave MWS 3+ system. The mass spectrometer operating conditions were as follows: radio frequency generator power—1300 W; cone material—platinum. All measurements were carried out in the mode of quantitative analysis constructing the calibration curves. Multi-element standard solutions certified were used to establish calibration dependencies. Certified samples of BCR-2 basalt and AGV-2 andesite (USGS) were used for control. For the analysis of a series of samples, the standard sample was measured at a frequency of 1:5–1:10. The obtained concentrations of rare, trace, and rare earth elements correspond to the certified values with an acceptable deviation of 15%. The errors in element determination were (relative %): 24 (Cr, Ni, Co, Cu, V, Ba, Sr), 30 (Rb), 41 (REE), 50 (Zr), and 60 (Y, Hf, Ta, Nb, Th, U).

Measurements of oxygen isotopic composition were carried out on a FINNIGAN MAT 253 gas mass spectrometer (Thermo Finnigan MAT GmbH, Bremen, Germany) at the "Geospektr" Center (GIN SB RAS, Ulan-Ude) using a double inlet system in the classical version (standard-sample). Sample preparation for determining $\delta^{18}O$ values was carried out using the laser fluorination (LF) method on the "laser ablation with oxygen extraction from silicates" option in the presence of BrF_5 reagent according to the method in [73]. Calculations were carried out relative to O_2 working standard, calibrated using the V-SMOW scale by means of regular measurements of oxygen according to the international standards NBS-28 (quartz) and NBS-30 (biotite). The accuracy of the obtained values was verified by regular measurements of GI-1 internal standard (quartz) and the Polaris laboratory standard (quartz) of IGEM RAS. The error in the obtained $\delta^{18}O$ values was (1σ) ± 0.2‰.

3. Results

3.1. Geology of Bikilyar Occurrence

The Bikilyar S-type nephrite occurrence is located on the top of Mount Bolshoy (Big) Bikilyar in the Filimonovo rural settlement of the Chebarkul' District of the Chelyabinsk Region, South Urals. Mount Bolshoy Bikilyar is located 10 km southwest of the village of Kundravy and rises above the surrounding terrain (Figures 2 and 5). It is 545 m high, and its coordinates are N 54°46′56″, E 60°5′33″.

The occurrence was discovered and described by A.A. Mamurovsky, an employee of the Lithogaea Petrographic Institute, in 1916 [18]. The occurrence was considered promising for the extraction of ornamental nephrite. However, as a result of the research carried out by Uralquartzsamotsvety in the 1970s and 1980s, the quality of nephrite was fond to be low, not meeting the requirements of the stone-cutting industry.

According to A.A. Mamurovsky [18], Mount Bolshoy Bikilyar is composed predominantly of altered gabbro, transformed into zoisite-albite-amphibole rock with relics of diopside. The mount is surrounded by serpentinite on three sides; granite is exposed on the northwestern slope, the veins of which cut through the serpentinite to the north of the mount. The nephrite occurrence is a cluster of large, dark green blocks [18], located at the top of Mount Bolshoy Bikilyar. Later, the blocks were apparently destroyed during revision work and/or unlicensed nephrite mining. A diopside rock with a small amount of zoisite is present, directly adjacent to the nephrite. At the contact, nephrite contains numerous grains of diopside, replaced by actinolite. The nephrite is gray-green, and uneven in hardness, translucency, and polishing ability. There are veins of transparent pure actinolite. The structure is tangled and fibrous–fascicular, and there are large and small bundles of

needles—small spindle-shaped and sheaf-shaped actinolite crystals. It is assumed that nephrite was formed after diopside schliere in gabbro under the influence of solutions that introduced MgO and FeO and removed CaO and Fe_2O_3 [18]. Schliere refers to a section of the gabbro intrusive that is highly enriched in diopside.

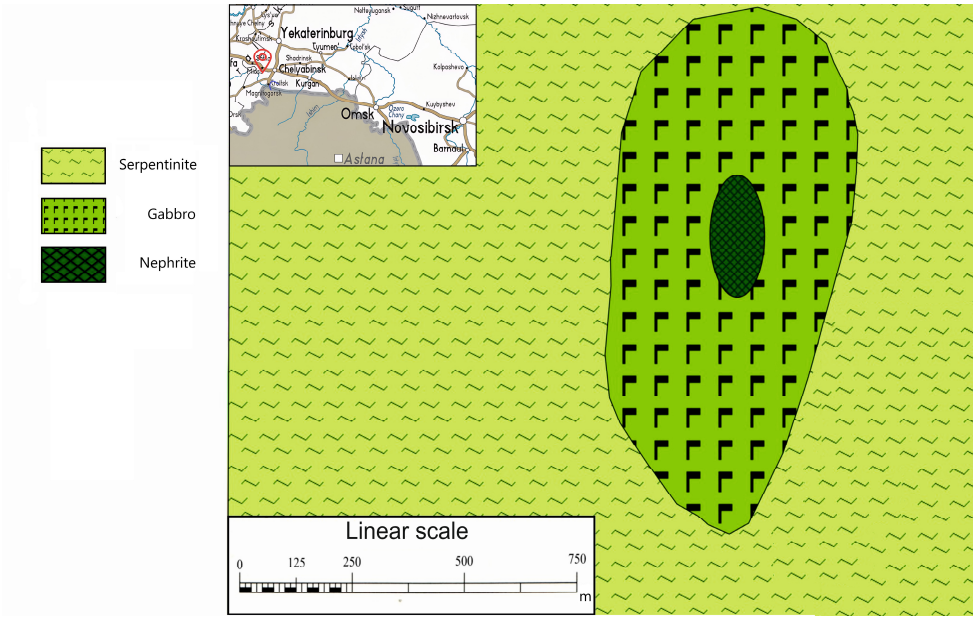


Figure 5. The geological map of Bikilar occurrence.

This occurrence is confined to the rocks of the Chebarkul–Kazbaev gabbro–dunite–harzburgite complex υσO2čk [74]. The rocks are represented mainly by after harzburgite antigorite serpentinites. The after dunite and pyroxenite serpentinite varieties are less common. Gabbro is formed by (vol. %) saussuritized labradorite (40–50), augite (10–25), uralite hornblende (25–50), accessory titanomagnetite (up to 2), sphene, apatite, and leucoxene. Metasomatites formed by ultramafic rocks are represented by talc-actinolite, talc-tremolite, talc-chlorite, talc-carbonate, and actinolite-tremolite rocks and rodingites. The complex formations are mainly metamorphosed under the conditions of greenschist and epidote-amphibolite facies. In terms of composition and petrogeochemical features, they correspond to the dunite–harzburgite ophiolite association [74].

3.2. Quality Characteristics of Nephrite

The color of the nephrite is heterogeneous and varies from gray to dark grassy green, with predominant shades of gray (Figure 3). The nephrite contains visually distinguishable grains of tremolite and diopside, streaks of needle-like actinolite, and dull spots of chlorite. Its translucency is to 1–2 mm. The nephrite shows a satisfactory, uneven polished (though slightly dull) surface, with a ubiquitous shagreen texture that ranges from fine to coarse. The quality of the nephrite is low, and it does not meet the requirements for high-grade stone.

3.3. Mineral Composition of Nephrite

Nephrite's composition is dominated by tangled fibrous to downy aggregates, and less often by large lamellar grains of actinolite (Figure 6). The composition of actinolite varies within narrow limits: 5.15–8.62 wt. % FeO, with rare admixtures up to 2.27 wt. % Al_2O_3, 1.26 wt. % Cr_2O_3, 0.54 wt. % Na_2O, and 0.19 wt. % Cl (Table 1, Supplementary Table S1). Occasionally, magnesian hornblende is observed in the actinolite aggregates, which is more typical for diopside-containing nephrite (Figure 6B,C, Table 1, Supplementary Table S1).

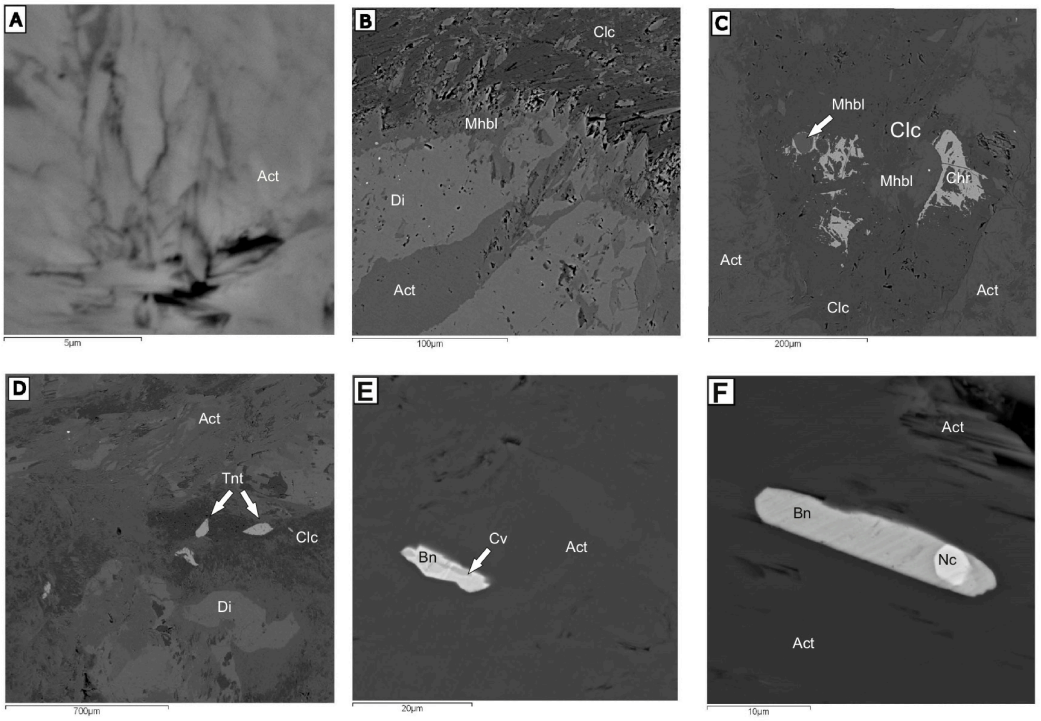


Figure 6. The relationship between nephrite minerals: (**A**)—tangled and fibrous structure of actinolite, B2; (**B**)—edge of the diopside grain, cross parallel veins of actinolite, magnesian hornblende and clinochlore fouling, B2; (**C**)—resorbed relict chromite grains with magnesian hornblende in a clinochlore isolation at actinolite aggregate, B1/1; (**D**)—actinolite with diopside relics replaced by clinochlore, idiomorphic titanite, B2; (**E**)—bornite with inclusions of covellite in actinolite, B1; (**F**)—elongated grain of bornite with rounded inclusions of nickeline in actinolite, B2. Act—actinolite, Bn—bornite, Chr—chromite, Clc—clinochlore, Cv—covellite, Di—diopside, Mhbl—magnesian hornblende, Nc—nickeline, Tnt—titanite [75]. The images were taken using a LEO-1430VP scanning electron microscope.

Table 1. Chemical composition of the nephrite minerals, wt. %.

	Actinolite n = 38		Magnesian Hornblende n = 8		Diopside n = 11	
	Range	Mean	Range	Mean	Range	Mean
SiO_2	53.93–57.57	56.30	42.87–52.03	49.54	51.69–54.68	52.80
TiO_2	-	-	0–1.22	0.15	0–0.43	0.10
Al_2O_3	0–2.27	0.52	5.42–13.60	7.52	0–3.00	2.07
Cr_2O_3	0–0.60	0.13	0–1.17	0.72	0–1.08	0.76
FeO	5.15–8.56	6.20	6.75–8.59	7.40	1.23–4.48	3.49
Fe_2O_3	-	-	-	-	0–2.97	0.71
MnO	-	-	0–0.32	0.08	0–0.36	0.06
MgO	19.09–21.43	20.40	15.48–18.34	17.41	15.77–17.38	16.80
CaO	13.19–13.99	13.57	12.27–13.42	13.10	20.61–25.55	22.64
Na_2O	0–0.54	0.06	0–3.15	1.15	0–0.43	0.08
K_2O	-		0–0.28	0.03	-	-
NiO	-	-	-	-	-	-
ZnO	-	-	-	-	-	-
V_2O_3	-	-	-	-	-	-
Cl	-	-	-	-	-	-

Table 1. *Cont.*

	Chromite n = 4		Titanite n = 3		Chlorite n = 26	
	Range	Mean	Range	Mean	Range	Mean
SiO_2	-	-	30.14–31.71	30.80	26.64–30.85	28.19
TiO_2	0–0.38	0.10	39.15–40.60	39.77	-	-
Al_2O_3	19.76–20.88	20.34	0.79–1.08	0.94	16.44–20.46	18.65
Cr_2O_3	40.03–41.74	40.64	-	-	0–4.25	1.54
FeO	30.30–31.73	30.81	0.39–0.77	0.60	10.68–13.71	11.54
Fe_2O_3	5.56–7.20	6.31	-	-	-	-
MnO	1.24–1.54	1.36	-	-	0–0.34	0.03
MgO	1.43–1.69	1.59	-	-	24.33–26.67	25.44
CaO	-	-	28.52–28.80	28.70	0–1.06	0.11
Na_2O	-	-	-	-	-	-
K_2O	-	-	-	-	-	-
NiO	-	-	-	-	0–0.51	0.04
ZnO	1.49–2.34	1.96	-	-	-	-
V_2O_3	0.35–0.51	0.47	-	-	-	-
Cl	-	-	-	-	-	-

Note: n—Number of analyses; the fully obtained results are shown in the Supplementary Files.

Diopside with various admixtures forms large, abundant resorbed grains in sample B2 (Figure 6B, Table 1, Supplementary Table S2). Relict corroded chromite outputs with admixtures of manganese, zinc and vanadium in chlorite aggregates were found in sample B1/1 (Figure 6C, Table 1, Supplementary Table S4). Idiomorphic grains of hydroxyapatite (Supplementary Table S5) are observed in sample B1, and titanite with an admixture of aluminum and iron in sample B2 (Figure 6D, Table 1, Supplementary Table S6). The chlorite formation is characteristic—clinochlore with an uneven content of Cr_2O_3 up to 4.25 wt. %, corroding diopside, chromite, and actinolite (Figure 6B–D, Table 1, Supplementary Table S3).

Small grains of bornite are common (Figure 6E,F, Ni admixture in 1 grain), while covellite (Figure 6E), chalcopyrite with Ni admixture, pentlandite with Co admixture, and sugakiite $Cu(Fe,Ni)_8S_8$ are less common, and there is a single inclusion of nickelite in bornite (Figure 6F). The chemical composition of sulfides is given in Supplementary Table S8. There are thin veins of chrysocolla and other secondary minerals in association with barite (Supplementary Table S9).

3.4. Mineral Composition of Metagabbro

The mineral composition of metagabbro is diverse. Green metagabbro with magnetite B3 (Figures 4A and 7C,D) is composed of aggregates of albite (Supplementary Table S9), chlorite (Supplementary Table S21), ilmenite (Supplementary Table S13), muscovite (Supplementary Table S17) and epidote (Supplementary Table S23), with metacrystals of magnetite (Supplementary Table S15) and muscovite, rare grains of rutile (Supplementary Table S18), pyrite (Supplementary Table S19), fluorapatite (Supplementary Table S11), monazite (Supplementary Table S16) and xenotime (Supplementary Table S14), goethite (Supplementary Table S12), and other secondary minerals (Supplementary Table S24).

Dark-colored metagabbro B4 (Figure 7C,D) is composed of granular, acicular, fibrous aggregates of amphibole (hornblende is slightly more abundant than actinolite; Supplementary Table S10), interstitial chlorite (Supplementary Table S21) and albite (Supplementary Table S9), as well as clinozoisite (Supplementary Table S23) metacrystals, euhedral titanite (Supplementary Table S20) grains, rare zircon (Supplementary Table S22), chalcopyrite, and covellite (both—Supplementary Table S19).

In light-colored metagabbro B5 (Figures 4B and 7E,F), there are predominantly granular, fan-shaped aggregates of actinolite, and, less often, hornblende (Supplementary Table S10), which also form layered aggregates with albite (Supplementary Table S9), and clinozoisite (sometimes predominating or forming large laths; Supplementary Table S23), titanite (Supplementary Table S20), and zircon (Supplementary Table S22) are also found.

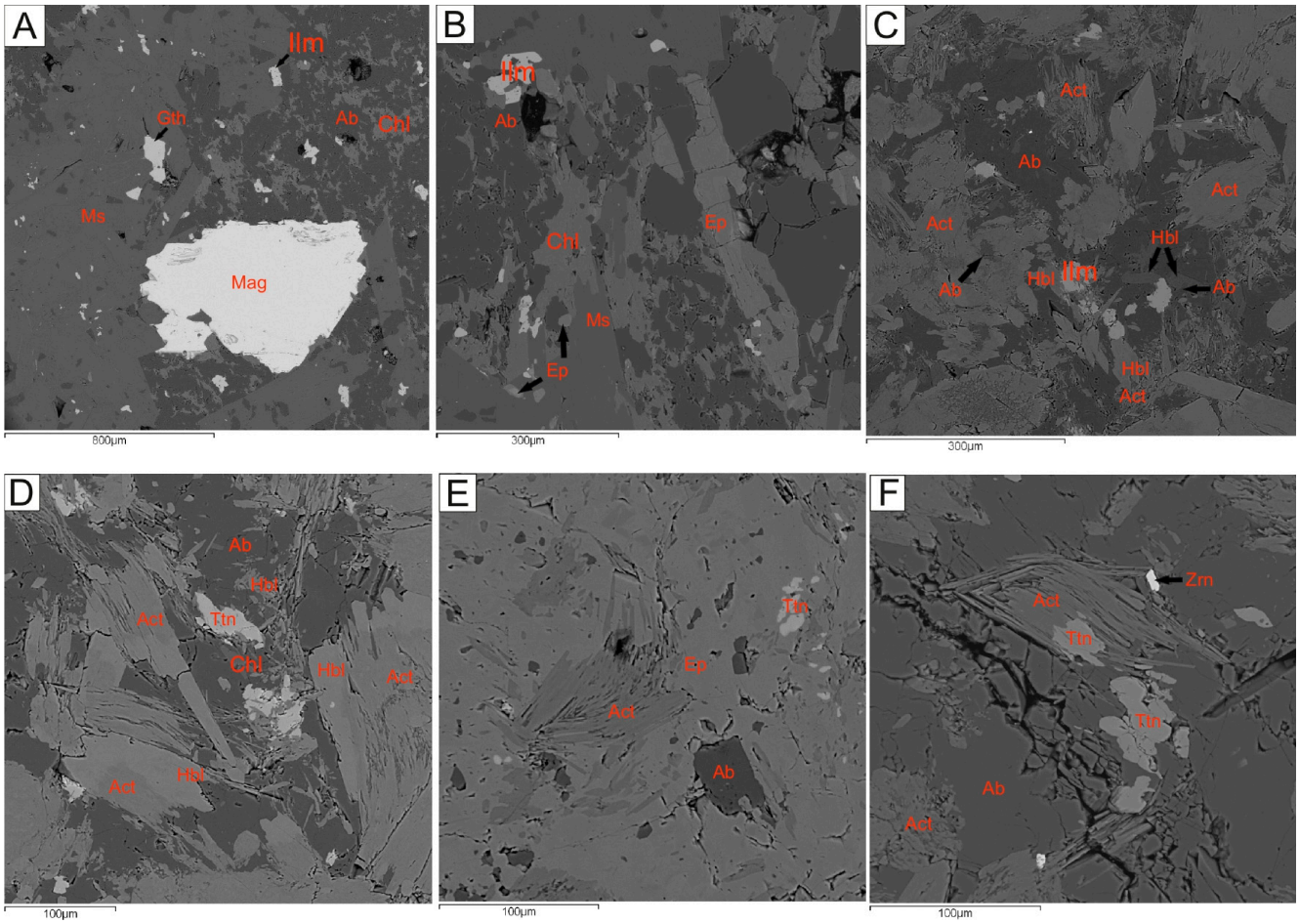


Figure 7. The ratio of metagabbro minerals: (**A**)—large magnetite grains, small grains are replaced by goethite; predominantly muscovite, chlorite, albite, and ilmenite, B3; (**B**)—elongated crystals of epidote, muscovite, chlorite, and albite, and isometric grains of ilmenite, B3; (**C**)—titanite, chlorite, albite, actinolite, hornblende, and epidote, B4; (**D**)—granular, needle-like, wavy actinolite and hornblende of different compositions, chlorite and titanite of smaller sizes, and interstitial albite, B4; (**E**)—wide-angle actinolite, isometric albite, and fine inclusions of titanite, and the bulk is epidote, B5; (**F**)—wavy actinolite in combination with grains of titanite and zircon, and the bulk is large actinolite and albite, B5. Ab—albite, Act—actinolite, Chl—chlorite, Ep—epidote, Gth—goethite, Hbl—hornblende, Ilm—ilmenite, Mag—magnetite, Ms—muscovite, Tnt—titanite, Zrn—zircon [75]. The images were taken using a LEO-1430VP scanning electron microscope.

3.5. Chemical Composition

The chemical composition of the nephrite and the metagabbro is given in Table 2.

Table 2. Chemical composition of samples, wt. %, iron group elements in ppm (horizontal components, vertical number of the sample).

	SiO_2	TiO_2	Al_2O_3	Fe_2O_3	FeO	MnO	MgO	CaO	Na_2O	K_2O	P_2O_5	losses	Сумма
Nephrite B1	52.60	0.02	2.90	1.63	6.08	0.09	20.76	12.08	0.16	0.03	<0.10	3.74	100.09
B1-1	53.00	0.03	3.10	1.09	6.16	0.09	21.20	11.50	0.24	0.02	<0.10	3.66	100.09
B1/1	50.00	0.02	5.10	0.52	6.24	0.10	22.12	10.50	0.19	0.03	<0.10	5.09	99.91
B1/1-1	50.00	0.03	5.10	0.43	6.12	0.09	22.28	10.29	0.21	0.02	<0.10	4.92	99.49
B2	53.00	0.10	2.90	0.42	5.52	0.10	21.96	12.12	0.17	0.02	<0.10	3.49	99.80
B2-1	52.20	0.16	3.70	0.69	5.44	0.11	20.70	13.33	0.30	0.03	<0.10	2.84	99.50
Metagabbro													
B3	47.70	1.17	18.60	7.16	9.12	0.24	4.03	0.77	5.00	1.64	<0.10	4.13	99.56
B3-1	45.80	1.32	18.80	6.80	10.76	0.22	4.90	0.48	5.30	1.17	0.10	4.47	100.12
B4	51.30	0.46	14.00	0.68	5.28	0.10	11.31	10.33	3.86	0.15	<0.10	2.51	99.98
B4-1	51.90	0.46	14.00	0.96	4.92	0.09	11.25	10.57	3.38	0.09	<0.10	2.07	99.69
B5	53.90	0.53	14.30	1.28	2.80	0.06	9.78	11.73	3.50	0.07	0.11	1.73	99.79
B5-1	51.50	0.58	17.50	1.54	2.36	0.06	7.65	12.92	3.22	0.06	0.14	2.18	99.71

	CO_2	S	F	$\sum Fe_2O_3$	Cr	V	Co	Ni	Cu
Nephrite B1	0.66	<0.10	0.32	8.38	>>500	30	93	1050	720
B1-1	-	-	-	7.93	>>500	30	96	1070	450
B1/1	0.66	<0.10	0.05	7.45	>500	40	85	900	178
B1/1-1	-	-	-	7.22	>>500	42	84	850	160
B2	0.66	<0.10	0.02	6.55	>500	65	95	800	160
B2-1	-	-	-	6.73	>>500	98	83	1030	650
Metagabbro									
B3	0.66	<0.10	0.02	17.28	26	300	35	11	346
B3-1	-	-	-	18.74	34	385	46	18	255
B4	0.66	<0.10	0.02	6.54	>500	190	43	200	6
B4-1	-	-	-	6.42	>>500	256	53	230	10
B5	0.44	<0.10	<0.02	4.39	>500	190	43	200	6
B5-1	-	-	-	4.16	340	200	27	165	5

3.6. Trace Elements

The results of the analysis are given in Table 3.

Table 3. Trace elements, ppm (horizontal number of the sample, vertical components).

	Nephrite			**Metagabbro**		
	B1	**B1/1**	**B2**	**B3**	**B4**	**B5**
Li	1.2	1.4	0.6	22	6	2.1
Be	0.039	0.06	0.05	0.9	0.1	0.06
Sc	5	8	27	80	50	40
Ti	80	90	400	4200	1500	1800
V	28	40	60	340	190	170
Cr	1130	2700	1800	27	430	170
Mn	340	360	400	1100	360	230
Co	66	60	54	34	30	20
Ni	600	500	400	7	110	100
Cu	340	130	80	230	6	6
Zn	18	24	20	120	18	13
Ga	1.7	2.4	1.7	22	7	7
Ge	0.9	0.9	1	1.6	0.9	0.9
As	1.06	1.3	0.76	1.7	0.54	0.58
Se	0.27	0.21	0.27	0.76	0.46	0.43

Table 3. *Cont.*

	Nephrite			Metagabbro		
	B1	**B1/1**	**B2**	**B3**	**B4**	**B5**
Rb	0.8	0.29	0.35	24	0.35	0.25
Sr	5	3.8	4	50	100	220
Y	1.1	0.7	3	11	13	14
Zr	0.5	0.5	1.5	30.6	23.9	25.1
Nb	0.023	0.022	0.033	1.2	0.5	0.7
Mo	0.21	0.17	0.14	1.3	0.29	0.28
Ag	0.085	0.047	0.0017	0.135	0.0036	0.0138
Cd	0.05	0.06	0.07	0.07	0.05	0.05
Sn	0.043	0.25	0.036	1.2	0.23	0.22
Sb	0.9	1.5	1	0.21	0.4	0.3
Te	0.07	<0.01	0.011	2	0.014	0.016
Cs	0.22	0.11	0.09	1.5	0.025	0.014
Ba	3.8	5.5	1.3	360	19	30
La	0.2	0.1	0.13	2.6	1.6	1.8
Ce	0.43	0.19	0.37	5	5	6
Pr	0.051	0.024	0.06	0.8	0.8	1.1
Nd	0.24	0.12	0.42	3.7	5	6
Sm	0.09	0.046	0.2	1.2	1.6	2
Eu	0.012	0.008	0.041	0.7	0.5	0.8
Gd	0.13	0.077	0.33	1.7	2.1	2.5
Tb	0.021	0.013	0.06	0.25	0.3	0.4
Dy	0.13	0.09	0.41	1.7	2.1	2.5
Ho	0.029	0.021	0.09	0.36	0.5	0.5
Er	0.09	0.07	0.26	1.1	1.4	1.6
Tm	0.014	0.012	0.035	0.18	0.2	0.22
Yb	0.11	0.09	0.22	1.4	1.3	1.4
Lu	0.019	0.017	0.03	0.23	0.19	0.2
Hf	0.014	0.014	0.05	0.8	0.7	0.8
Ta	0.0035	0.0031	0.003	0.05	0.03	0.05
W	0.26	0.3	0.4	3.4	0.4	0.6
Tl	0.003	0.005	0.0032	0.09	0.005	0.0031
Pb	1.5	2.3	0.8	6	0.8	1.2
Bi	0.086	0.033	0.064	4	0.076	0.135
Th	0.023	0.018	0.013	0.3	0.3	0.3
U	0.08	0.013	0.028	0.38	0.18	0.24

The nephrite is characterized by a subchondrite trough-shaped distribution spectrum of rare earth elements with a negative Europium anomaly. The metagabbro spectrum normalized after chondrite C1 is characterized by significantly higher REE contents, and sample B3 has a positive Europium anomaly (Figure 8).

3.7. $\delta^{18}O$ Isotopic Composition

The $\delta^{18}O$ isotopic composition of the nephrite varies slightly from +5.53 to +5.80‰ (Table 4). The metagabbro is characterized by wide variations with a generally heavier composition of +4.42 to +11.27‰, especially in green metagabbro B3.

Table 4. Isotope composition of the samples, ‰.

	δ^{18}O V-SMOW
Nephrite	
B1	+5.71
B1/1	+5.80
B2	+5.53
Metagabbro	
B3	+11.27
B4	+7.09
B5	+4.42

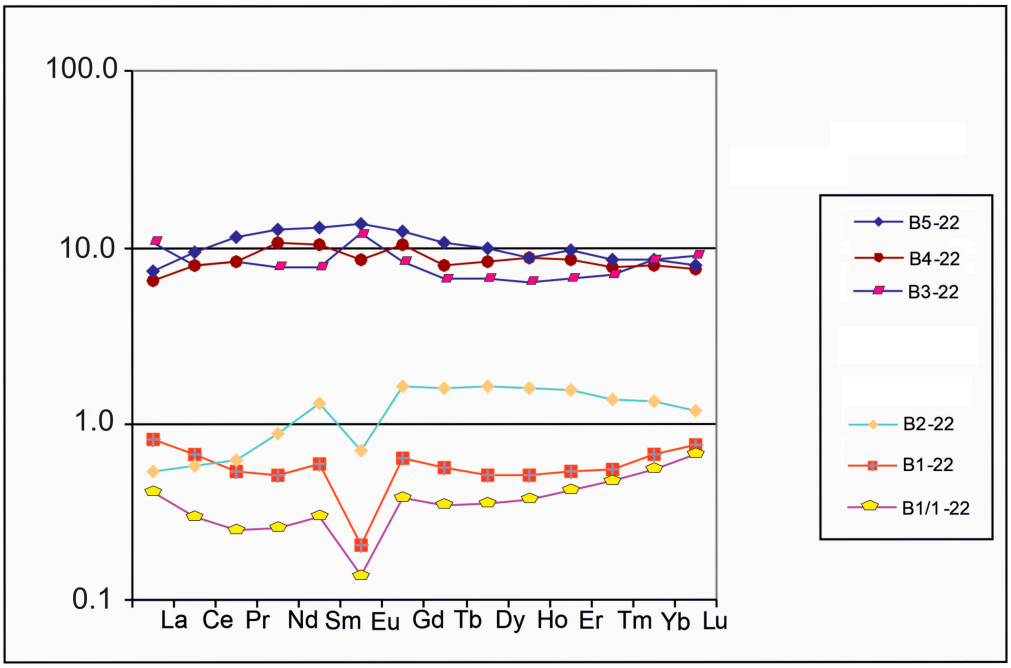


Figure 8. Normalized spectra of rare earth element contents of nephrite B1, B1/1, and B2 and metagabbro B3, B4, and B5.

4. Discussion

The Bikilyar nephrite differs in its mineral composition from the S-type nephrite of other deposits in the Urals—Akademicheskoe and the accompanying occurrences in the Miass region in the Southern Urals [23,24], Nyrdvomenshor in the Subpolar Urals [20] and the Bazhenov chrysotile–asbestos deposit in the Middle Urals [22]. The nephrite of these deposits is composed of tremolite and is characterized by the widespread development of grossular-uvarovite garnet. At the same time, magnesian hornblende, titanite, and apatite are not observed, while sulfides are found only at the Miass deposits. The Bikilyar nephrite is composed mainly of actinolite and titanite, due to the predominance of gabbro, which contains significantly more iron and titanium (Table 2) than the ultramafic xenoblock rocks.

The green metagabbro with magnetite B3 resembles the chloritolites uncovered in the raft of the Mokhovoye Boloto gold placer in the Southern Urals [76]; it is assumed that they were formed by the metasomatic replacement of dolerite dike of the Chebarkul–Kazbaev complex.

Despite the unique mineral composition, the chemical composition of the Bikilyar nephrite is typical of the S-type: FeO/(MgO + FeO) wt. % value varies from 0.20 to 0.22; Cr content is significantly greater than 500 ppm, Co—83–96 ppm, and Ni—800–1070 ppm by the atomic emission spectral method; Cr 1130–2700 ppm, Co—54–66 ppm, Ni—

400–600 ppm by ICP-MS. The F content is 0.02–0.32 wt. %, 0.13 wt. % on average. The Ba-to-Sr ratio is less than one in two samples.

The S-type nephrite was specified according to its chemical composition. It is believed that the S-type nephrite has typical values of $Fe^{2+}/(Mg + Fe^{2+}) > 0.06$, whereas for the dolomite-type nephrite it is <0.06 [77]. The content range is different for Russian deposits. For S-type nephrite on average, the following composition is typical: Ospa—4.12 wt. % FeO, 21.89 wt. % MgO (23 samples); Gorlykgol—3.28 wt. % FeO, 22.73 wt. % MgO (8); Zyn-Ospa—4.38 wt. % FeO, 22.86 wt. % MgO (1); Bortogol—2.58 wt. % FeO, 22.74 wt. % MgO (2); Ulankhoda—3.30 wt. % FeO, 22.79 wt. % MgO (22); Khokhyurta—3.50 wt. % FeO, 21.67 wt. % MgO (3); (1); Khamarkhuda—5.30 wt. % FeO, 20.19 wt. % MgO (1); Kurtushiba—3.17 wt. % FeO, 22.99 wt. % MgO (3); Param—4.12 wt. % FeO, 22.27 wt. % MgO (18); Yangoza—6.91 wt. % FeO, 20.26 wt. % MgO (2) [3]; Bazhenov—3.76 wt. % $Fe_2O_{3\sum}$, 22.81 wt. % MgO (3) [22], Nyrdvomenshor—5.27 wt. % $Fe_2O_{3\sum}$, 21.62 wt. % MgO (3) [20].

The content of Cr, Ni, and Co in the nephrite can also be used to distinguish the S-type and dolomite-type nephrite [77]. The Cr (900–2812 ppm), Ni (958.7–1898 ppm) and Co (42–207 ppm) contents in the S-type nephrite are relatively high, while the Cr (2–179 ppm), Ni (0.05–471 ppm) and Co (0.5–10 ppm) contents in the dolomite-type nephrite are relatively low [68,77–79].

The content range is wider for Russian deposits. For S-type nephrite on average, the following composition is typical: Ospa deposit—1170 ppm of Cr, 1020 ppm of Ni, 65 ppm of Co (16 samples); Gorlykgol—270 ppm, 1050 ppm, 97 ppm (3); Bortogol—580 ppm, 100 ppm, 53 ppm (3); Ulankhoda—1200 ppm, 1400 ppm, 62 ppm (26); Kitoy—30 ppm, 120 ppm, 5 ppm (1); Khamarkhuda—660 ppm, 590 ppm, 54 ppm (32); Param—1500 ppm, 1250 ppm, 64 ppm (8); Kelyana—1700 ppm, 1800 ppm, 56 ppm (1); Kurtushiba—970 ppm, 1230 ppm, 61 ppm (3); Agardak—1100 ppm, 420 ppm, 42 ppm (1); Khalilov—180 ppm, 600 ppm, 22 ppm (10); Kozmodemyanov—800 ppm, 900 ppm, 50 ppm (1), Nyrdvomenshor—1110 ppm, 570 ppm, 68 ppm (7) [3], 513 ppm, 400 ppm, 23 ppm [20].

The fluorine content in S-type nephrite is significantly lower than in dolomite-type nephrite; on average for deposits, the composition is as follows: Ospa—0.04 wt. %, Ulankhoda—0.04 wt. %, Nyrdvomenshor—0.01 wt. %, Khamarkhuda—0.07 wt. % [3]. The indicator elements can also include barium and strontium. In contrast to the dolomite-type nephrite, with strontium-to-barium ratios of 1.7–2.0, in S-type nephrite, the strontium–barium ratio is less than 1 or slightly higher [3].

The differences in REE content between the nephrite and the metagabbro demonstrate that the hypothesis of A.A. Mamurovsky [18], according to which the diopside schliere in gabbro constitutes the nephrite protolith, is incorrect. The contents and distribution of REE in gabbro and diopside schliere should be similar. In the case that the nephrite was formed after diopside shliere, it likely inherited the contents and nature of distribution of REE, which was not observed.

The isotopic composition $\delta^{18}O$ of nephrite being +5.53 to +5.80‰ indicates that the oxygen content was inherited from ultramafic rocks involved in low-temperature hydrothermal processes, determining the isotopic composition. The typical oxygen isotopic composition of ultramafic rocks is +5.4 to +6.6‰ [80]. The extremely heterogeneous and heavier composition of the metagabbro of +4.42 to +11.27‰ does not correspond to the usual data for gabbro of +5.5 to +7.4‰ [80]. Such compositions are explained by metamorphic and metasomatic processing and do not show that the nephrite inherited metagabbro characteristics.

The oxygen isotopic composition was determined for a number of S-type nephrite deposits in Russia: Param in Vitim, +6.13 to +9.54‰; Ospa in the Eastern Sayan +8.43‰; and Hamarkhuda in Dzhida +6.72 to +7.87‰. It is believed that the fluid phase of nephrites indicates their transformation from serpentinites during metamorphism [81]. Later, the

authors determined the isotopic composition of ultramafic rocks in the following deposits: dunite of Ospa +4.60‰ and Gorlyk-Gol 5.50‰, serpentinite of Ospa +4.67 to +7.35‰, and Param +6.91 to +7.05‰. Quartz from listwanite in Ospa showed values of +12.82 to +17.46‰, and talc – +8.12 to +12.65‰. Quartz from Ospa granite showed a value of +13.70‰, and feldspar – +11.40‰ [82]. The oxygen isotopic composition of serpentinites is inherited from ultramafic rocks and indicates the juvenile origin of their fluids. The fluid phase of the nephrites was mobilized from serpentinites with the addition of some part of the crustal component [82].

The oxygen isotopic composition of the nephrite was studied at the localities of the Eastern Sayan: Ara-Khushan-Zhalga +5.02 to +6.64‰, Bortogol +3.89 to +5.92‰, Gorlyk-Gol +4.80 to +7.09‰, Ospa +5.46 to +8.04‰, Ulan-Khoda +5.46 to +8.04‰, and Dzhida: Hamarhuda +6.67 to +11.76‰, Kharganta +11.00 to +11.49‰, Khokhyurta +6.45‰, and Boldokit +5.21 to 8.22‰ [83]. The nephrites of the Nyrdvomenshor deposit in the Polar Urals have an isotopic composition of +8.2 to +9.7‰. This indicates the contribution of crustal fluids to ultramafic rocks [20].

At the Fengtien deposit in Taiwan, for ordinary nephrite, the oxygen isotope composition is +4.5 to +5.3‰; for wax-like nephrite, it is +4.7 to +5.0‰; and for nephrite with the "cat's eye" effect, it is +5.1 to +5.3‰. It is concluded that nephrite inherits its composition from serpentinites [38]. The oxygen isotope composition was determined at Xinjiang deposits: Manas +9.10 to +12.20‰ [28], Hetian-Yutian +4.10 to +9.10‰ [29], Qiemo +15.30 to +15.40‰ [30].

At the Jordanov deposit in Poland, the oxygen isotope composition is +6.1‰, and for the shale nephrite, it is +6.7‰ [60]. The oxygen isotope composition for the S-type nephrite in the Chinese province of Qinghai is +8.1 to +8.6‰; in Russia, it is +8.2 to +8.5‰; in Canada, it is +9.4 to +12.3‰; in New Zealand, it is +4.7 to +8.0‰; in Australia, it is +1.3 to +1.6‰; and in Pakistan, it is +13.0 to +13.4‰. It is shown that ore-forming fluids are formed as a result of metamorphism [84]. Single analyses were performed for S-type nephrite from the Chara Dzhelgra River in Siberia (+6.9‰), Red Mountain in New Zealand (+7.5‰), Mount Ogden, Canada (+9.6‰), and the Shulaps Range, Canada (+8.4‰). These values are explained by the inheritance of the isotopic composition of the initial serpentinite with the possible influence of its contact with metagabbro or crystalline shales [85].

Thus, the oxygen isotope composition of Mount Bikilar nephrite is quite typical of the S-type nephrite. And the features of this composition are explained as inheritance from ultramafic rocks with deviations due to interaction with intrusive or other aluminosilicate rocks by all researchers.

To understand the mechanism of the nephrite formation during the interaction of the intrusive gabbro with the ultramafic xenoblock, the chemical composition of the source rocks and the nephrite can be analyzed. The chemical composition of the Chebarkul–Kazbaev complex serpentinite corresponds to: SiO_2 37.62–41.85 wt. %, TiO_2 wt. 0–0.04%, Al_2O_3 0.70–0.91 wt. %, Fe_2O_3 3.69–6.87 wt. %, FeO 1.18–3.43 wt. %, MgO 37.46–37.67 wt. %, CaO 0–0.38 wt. %, Na_2O 0.12–0.25 wt. %, losses 11.46–13.93 wt. % [86]. The chemical composition of the gabbro from the same complex differs sharply (averaging of five analyses): SiO_2 47.59 wt. %, TiO_2 0.27 wt. %, Al_2O_3 15.87 wt. %, Fe_2O_3 2.13 wt. %, FeO 4.49 wt. %, MgO 10.14 wt. %, CaO 14.56 wt. %, Na_2O 1.17 wt. %, losses 2.70 wt. % [86]. The chemical composition of the studied nephrite is given in Table 2, with intermediate values: SiO_2 50.00–53.00 wt. %, TiO_2 wt. 0.02–0.16 wt. %, Al_2O_3 2.90–5.10 wt. %, Fe_2O_3 0.42–1.63 wt. %, FeO 5.44–6.24 wt. %, MgO 20.70–22.28 wt. %, CaO 10.29–13.33 wt. %, Na_2O 0.16–0.30 wt. %, losses 2.84–5.09 wt. %. This shows that the gabbro affected serpentinite both thermodynamically, providing the temperature necessary for metasomatosis and water loss, and by introducing the components necessary for metasomatosis—SiO_2, TiO_2, Al_2O_3, CaO, and Na_2O.

The mineral composition reveals a complicated formation history of nephrite involving a combination of tectonic and metasomatic processes. The tectonic stresses caused the rocks to be crushed, which facilitated penetration of the fluid and ensured the formation of a cryptocrystalline tangled fibrous structure of the nephrite.

At the progressive stage, serpentine is replaced by diopside:

$$(Mg, Fe)_3Si_2O_5(OH)_4 + 3Ca^{2+} + 4Si^{4+} + 5.5O_2 \rightarrow 3Ca(Mg, Fe)Si_2O_6 + 2H_2O.$$

Fluids containing calcium and silica come from gabbro.

At the regressive stage, diopside is replaced by an actinolite aggregate—nephrite:

$$2Ca(Mg, Fe)Si_2O_6 + Mg^{2+} + 4Si^{4+} + H_2O + 5.5O_2 \rightarrow Ca_2(Mg, Fe)_5[Si_4O_{11}]_2(OH)_2.$$

This is indicated by relic grains of diopside.

As the retrogressive process continues, chlorite replaces both tremolite and diopside, which have worsened the quality of the nephrite:

$$Ca_2(Mg, Fe)_5[Si_4O_{11}]_2(OH)_2 + Al^{3+} + 3H_2O \rightarrow (Mg, Fe)_5Al[Si_3AlO_{10}](OH)_8 + 2Ca^{2+} + SiO_2 + 3.5O_2.$$

$$5Ca(Mg, Fe)Si_2O_6 + Al^{3+} + 4H_2O + 5O_2 \rightarrow (Mg, Fe)_5Al[Si_3AlO_{10}](OH)_8 + 5Ca^{2+} + 2SiO_2.$$

The quality of the nephrite is low, and it does not meet the requirements for raw gemstone material. The yield of high-grade stone suitable for stone-cutting or decorative tiles is limited. The Bikilyar locality is hopeless in terms of nephrite mining. But it is attractive, given the historical significance of being one of the first sites of nephrite finds in the Urals. In addition, it is located in the popular tourist area of the Ilmen Reserve and resort lakes. Therefore, it is recommended as a natural monument and tourist attraction [87,88]. Sampling by tourists will not lead to the destruction of the monument.

5. Conclusions

Nephrite of the Bikilyar locality differs from the nephrite of other deposits and localities of the Urals in terms of the localization and composition of its minerals. The studied nephrite contains actinolite, magnesian hornblende, titanite, and hydroxyapatite. The composition of rare earth elements of the nephrite and the host metagabbro is different, which does not confirm the formation of the nephrite after diopsidite schliere in gabbro. The oxygen isotopic composition of the nephrite also differs from that of metagabbro, being inherited from ultramafic rocks. This indicates that the nephrite was formed by an ultramafic xenoblock under the influence of an enclosing gabbro. The specificity of the mineral composition is a consequence of the small size of this xenoblock compared to the significant volume of gabbro, which hosts and transforms it. During nephrite formation, serpentine was initially replaced by diopside, which led to the development of actinolite, to then form nephrite. Subsequently, relict chromite and diopside, as well as actinolite, were replaced by chlorite, in addition to the hydrothermal deposition of sulfides, and, later, the formation of barite and chrysocolla. The quality of the nephrite is low, and it does not meet the requirements for raw gemstone material. It is recommended that Bolshoy Bikilyar Mountain is considered a natural monument and tourist attraction.

Supplementary Materials: The following supporting information can be downloaded at https://www.mdpi.com/article/10.3390/min16080818/s1: Table S1: Chemical composition of amphiboles of nephrite; Table S2: Chemical composition of diopside from nephrite B2; Table S3: Chemical composition of chlorite of nephrite; Table S4: Chemical composition of chromite from nephrite B1/1; Table S5: Chemical composition of hydroxyapatite from nephrite B1; Table S6: Chemical composition

of titanite from nephrite B2; Table S7: Chemical composition of sulfides from nephrite; Table S8: Chemical composition of barite and secondary minerals from nephrite B1; Table S9: Chemical composition of albite from metagabbro; Table S10: Chemical composition of amphiboles from metagabbro; Table S11: Chemical composition of apatite from metagabbro B3; Table S12: Chemical composition of goethite from metagabbro B3; Table S13: Chemical composition of ilmenite from metagabbro B3; Table S14: Chemical composition of xenotime from metagabbro B3; Table S15: Chemical composition of magnetite from metagabbro B3; Table S16: Chemical composition of monazite from metagabbro B3; Table S17: Chemical composition of muscovite from metagabbro B3; Table S18: Chemical composition of rutile from metagabbro B3; Table S19: Chemical composition of sulfides from metagabbro; Table S20: Chemical composition of titanite from metagabbro B4; Table S21: Chemical composition of chlorite of metagabbro; Table S22: Chemical composition of zircon of metagabbro; Table S23: Chemical composition of epidote group minerals of metagabbro; Table S24: Chemical composition of secondary minerals from metagabbro B3.

Author Contributions: Conceptualization, E.V.K.; methodology, E.V.K. and V.V.M.; validation, E.V.K. and V.V.M.; formal analysis, E.V.K. and V.V.M.; investigation, E.V.K. and V.V.M.; resources, V.V.M.; data curation, E.V.K.; writing—original draft preparation, E.V.K.; writing—review and editing, E.V.K. and V.V.M.; visualization, E.V.K. and V.V.M.; supervision, E.V.K.; project administration, E.V.K.; funding acquisition, E.V.K. All authors have read and agreed to the published version of the manuscript.

Funding: The research was carried out at the expense of the grant of the Russian Science Foundation No. 25-27-00579.

Data Availability Statement: The data supporting the reported results can be found in the Supplementary Files and can be provided by the corresponding author upon request.

Acknowledgments: The authors are grateful to the editor and three editorial board reviewers for comments and suggestions that significantly improved the manuscript of the article, to M.G. Egorova, D.V. Kiseleva, O.V. Korsun, B.B. Lygdenova, V.F. Posokhov, E.D. Utina, E.A. Khromova, E.V. Khodyreva, and T.G. Khumaeva for performing the analyses, and to V.Yu. Baryshnikova, A.E. Kislov, V.F. Sotnikova, A.V. Trofimov, and D.M. Wurms for assistance in the research. The analyses were performed using the equipment of the CCP "Geospectr" (GIN SB RAS, Ulan-Ude); trace elements were determined using the equipment of the CCP "Geoanalytik" (IGG UrB RAS, Yekaternburg). The work was carried out within the framework of the topic of the research work of GIN SB RAS 126020216342-3 and IGG UrB RAS 123011800011-2.

Conflicts of Interest: The authors declare no conflicts of interest. The funders had no role in the design of the study; in the collection, analyses, or interpretation of the data; in the writing of the manuscript; or in the decision to publish the results.

References

1. Kievlenko, E.Y. *Geology of Gems*; Ocean Pictures Ltd: Littleton, CO, USA, 2003; 468p.
2. Péterdi, B.; Szakmány, G.; Judik, K.; Dobosi, G.; Kasztovszky, Z.; Szilágyi, V.; Maróti, B.; Bendõ, Z.; Gil, G. Petrographic and geochemical investigation of a stone adze made of nephrite from the Balatonõszöd—Temetõi dûlõ site (Hungary), with a review of the nephrite occurrences in Europe (especially in Switzerland and in the Bohemian Massif). *Geol. Quart.* **2014**, *58*, 181–192. [CrossRef]
3. Suturin, A.N.; Zamaletdinov, R.S.; Sekerina, N.V. *Deposits of Nephrite*; IGU Publishing House: Irkutsk, Russia, 2015; 377p. (In Russian)
4. Barnes, G.L. Understanding Chinese jade in a world context. *J. Brit. Acad.* **2018**, *6*, 1–63. [CrossRef]
5. Nemeth, K.; Sági, T.; Józsa, S. Why the pounamu? Low- to medium grade metabasites and metaultrabasites of New Zealand from a geoheritage perspective. In *Metamorphic Rocks as Key to Understand Geodynamic Processes*; IntechOpen: Rijeka, Croatia, 2024; pp. 1–18. [CrossRef]
6. Harlow, G.E.; Sorensen, S.S. Jade (Nephrite and Jadeitite) and Serpentinite: Metasomatic Connections. *Int. Geol. Rev.* **2005**, *47*, 113–146. [CrossRef]
7. Sotnikova, V.F.; Sungatullin, R.K.; Kislov, E.V. First Mineralogical and Geochemical Data on Placer Nephrite in the Vitim Highland, Republic of Buryatia. *Lithol. Miner. Resour.* **2025**, *60*, 333–345. [CrossRef]

8. The State Balance of Mineral Reserves of the Russian Federation as of January 1, 2025. *Issue 79. Colored Stones*; FSBI Rosgeolfond: Moscow, Russia, 2025; 298p. (In Russian)
9. Zyryanova, L.A.; Chernyshov, A.I.; Senkin, O.A.; Trifonov, V.A.; Golubitskaya, I.N. Decorative, artistic and technological properties of nephrite occurences of the Katun ridge spurs (Maintain Altai). In *Gemology*; Tomsk CSTI: Tomsk, Russia, 2006; pp. 48–52. (In Russian)
10. Gusev, A.I. *Gemology of Altai with the Basics of Gemmotourism: A Textbook for University Students*; V.M. Shukshin BPSU: Biysk, Russia, 2007; 155p. (In Russian)
11. Rychkov, V.M.; Senkin, O.A.; Rychkova, S.I. Nephrites, rodingites, jadeites of Altai and Siberia. In *Natural Resources of Maintain Altai*; IP Vysotskaya G.G.: Gorno-Altaysk, Russia, 2012; pp. 78–91. (In Russian)
12. Gadiyatov, V.G.; Marshintsev, V.K. *Colored Stones of Yakutia and Their Deposits*; Cultural Information Bank: Yekaterinburg, Russia, 2000; 328p. (In Russian)
13. Krylova, G.I.; Kokarev, G.N.; Smirnov, A.A.; Shulyaeva, L.N. Occurences of colored stones in the Kuyulsky ultramafic massif. In *Issues of Mineralization in Ultramafics*; Nauka: Moscow, Russia, 1985; pp. 117–125. (In Russian)
14. Belyaev, E.V.; Antonov, V.A.; Polyanin, V.S.; Shcherbakova, T.A.; Miroshnikov, K.E. New types of mineral raw materials of the North Caucasus. *Miner. Resour. Russ. Econ. Manag.* **2016**, *6*, 16–21. (In Russian)
15. Polyanin, V.S.; Dusmanov, E.N.; Polyanina, T.A.; Yakovleva, E.I. About the first discovery of nephrite in the Caucasus. *Prospect Prot. Miner. Resour.* **2017**, *4*, 15–17. (In Russian)
16. Gazeev, V.M.; Gurbanov, A.G.; Gurbanova, O.A.; Popov, S.V. Collectible minerals and ornamental stones in ultrabasites and basites of the North Caucasus. *Bull. Vladikavkaz Sci. Cent.* **2018**, *18*, 29–35. (In Russian)
17. Krotov, B.P. Petrographic description of the southern part of the Miass dacha. *Proc. Soc. Nat. Sci. Kazan Univ.* **1915**, *47*, 1–402. (In Russian)
18. Mamurovsky, A.A. *The Nephrite Deposit on Mount Bikilyar*; Litogea: Moscow, Russia, 1918; 52p. (In Russian)
19. Kazak, A.P.; Dobretsov, N.L.; Moldavantsev, Y.E. Glaucophane schists, jadeites, vesuvianites and nephrites of the Rai-Iz hyperbasite massif. *Sov. Geol. Geophys.* **1976**, *17*, 50–55. [CrossRef]
20. Kislov, E.V.; Popov, M.P.; Nurmukhametov, F.M.; Posokhov, V.F.; Vanteev, V.V. Nyrdvomenshor Nephrite Deposit, Polar Urals, Russia. *Minerals* **2023**, *13*, 767. [CrossRef]
21. Yushkin, N.P.; Ivanov, O.K.; Popov, V.A. *Introduction to the Topominerology of the Urals*; Nauka: Moscow, Russia, 1986; 295p. (In Russian)
22. Kislov, E.V.; Erokhin, Y.V.; Popov, M.P.; Nikolayev, A.G. Nephrite of Bazhenovskoye Chrysotile-Asbestos Deposit, Middle Urals: Localization, Mineral Composition, and Color. *Minerals* **2021**, *11*, 1227. [CrossRef]
23. Arkhireev, I.E.; Maslennikov, V.V.; Makagonov, E.P.; Kabanova, L.Y. South Ural nephrite province. *Prospect Prot. Miner. Resour.* **2011**, *3*, 18–22. (In Russian) [CrossRef]
24. Makagonov, E.P.; Archireev, I.E. Nephrite of the Urals. *Geoarchaeology Archaeol. Mineral.* **2014**, *1*, 15–19. (In Russian) [CrossRef]
25. Knyazev, Y.G.; Knyazeva, O.Y.; Snachev, V.I.; Zhdanov, A.V.; Karimov, T.R.; Aidarov, E.M.; Masagutov, R.H.; Arslanova, E.R. *State Geological Map of the Russian Federation. Scale 1:1,000,000 (Third Generation). Seria Uralian. Sheet N-40–Ufa. Explanatory Note*; Cartographic factory VSEGEI: St. Petersburg, Russia, 2013; 512p. (In Russian)
26. Zhang, C.; Yang, F.; Yu, X.; Liu, J.; Carranza, E.J.M.; Chi, J.; Zhang, P. Spatial-temporal distribution, metallogenic mechanisms and genetic types of nephrite jade deposits in China. *Front. Earth Sci.* **2023**, *11*, 1047707. [CrossRef]
27. Tang, Y.L.; Liu, D.Q.; Zhou, R.H. Geological characteristics of Manasi green jade in Xinjiang. *Acta Petrol. Mineral.* **2002**, *9*, 22–25. (In Chinese)
28. Wan, D.F.; Wang, D.P.; Zou, T.R. Silicon and oxygen isotopic compositions of Hetian jade, Manasi green jade and Xiuyan old jade (tremolite). *Acta Petrol. Mineral.* **2002**, *21*, 110–114. (In Chinese)
29. Shi, M.; Yu, B.S.; Guo, Y.; Yuan, Y.; Ng, Y.N. Structural and mineralogical characterization of green nephrite in Hetian, Xinjiang, China. *Key Eng. Mat.* **2015**, *633*, 159–164. [CrossRef]
30. Jia, Y.H.; Liu, X.F.; Liu, Y.; Zhang, Q.C.; Zhang, Y.; Li, Z.J. Petrogenesis of the serpentinite-related nephrite deposit in Qiemo county, Xinjiang. *Acta Petrol. Mineral.* **2018**, *37*, 824–838. (In Chinese)
31. Wang, J.; Shi, G. Comparative Study on the Origin and Characteristics of Chinese (Manas) and Russian (East Sayan) Green Nephrites. *Minerals* **2021**, *11*, 1434. [CrossRef]
32. Yu, H.Y.; Wang, R.C.; Guo, J.C.; Li, J.G.; Yang, X.W. Study of the minerogenetic mechanism and origin of Qinghai nephrite from Golmud, Qinghai, Northwest China. *Sci. China Earth Sci.* **2016**, *59*, 1597–1609. [CrossRef]
33. Zhang, C.; Yu, X.; Yang, F.; Santosh, M.; Huo, D. Petrology and geochronology of the Yushigou nephrite jade from the North Qilian Orogen, NW China: Implications for subduction-related processes. *Lithos* **2021**, *380–381*, 105894. [CrossRef]
34. Jin, X.; Qiu, Z.; Dai, S.; Yi, J.; Li, L.; Zhang, Y. Gemmological and mineralogical characteristic of nephrite from Ya'an, Sichuan province. *J. Gems Gemol.* **2014**, *16*, 1–8. (In Chinese with English abstract)
35. Huang, C.K. Nephrite and blue chalcedony from Taiwan. *Proc. Geol. Soc. China.* **1966**, *9*, 11–19.

36. Wan, H.M.; Yeh, C.L. Uvarovite and grossular from the Fengtien nephrite deposits, Eastern Taiwan. *Mineral. Magaz.* **1984**, *48*, 31–37. [CrossRef]
37. Yui, T.-F.; Yeh, H.-W.; Lee, C.W. Stable isotope studies of nephrite deposits from Fengtien, Taiwan. *Geochim. Cosmochim. Acta* **1988**, *52*, 593–602. [CrossRef]
38. Yui, T.-F.; Usuki, T.; Chen, C.-Y.; Ishida, A.; Sano, Y.; Suga, K.; Iizuka, Y.; Chen, C.-T. Dating thin zircon rims by NanoSIMS: The Fengtien nephrite (Taiwan) is the youngest jade on Earth. *Int. Geol. Rev.* **2014**, *56*, 1932–1944. [CrossRef]
39. Umar, Z.A.; Liaqat, U.; Ahmed, R.; Baig, M.A. Classification of Nephrite Using Calibration-Free Laser Induced Breakdown Spectroscopy (CF–LIBS) with Comparison to Laser Ablation-Time-of-Flight-Mass Spectrometry (LA–TOF–MS). *Anal. Lett.* **2019**, *53*, 203–216. [CrossRef]
40. Rehman, H.U.; Bilal, O.S.; Rahman, O.U.; Shen, A.H. Namak Mandi: A pioneering gemstone market in Pakistan. *Gems Gemol.* **2021**, *57*, 138–149. [CrossRef]
41. Khan, R.A.; Anwar-ul-Haq, M.; Qasim, M.; Afgan, M.S.; Haq, S.U.; Hussain, S.Z. Spectroscopic and crystallographic analysis of nephrite jade gemstone using laser induced breakdown spectroscopy, Raman spectroscopy, and X-ray diffraction. *Heliyon* **2022**, *8*, e11493. [CrossRef] [PubMed]
42. Khan, A.; Shah, M.T.; Ali, L.; Alam, S.F.; Islam, I.; Khattak, S.A. Mineralogy and geochemistry of nephrite from Drosh area, district Chitral, northern Pakistan. *Ore Energy Res. Geol.* **2025**, *19*, 100115. [CrossRef]
43. Jan, M.Q.; Ullah, R.; Anjum, M.N. Magmatic (Cr-Ni-PGE) and secondary/hydrothermal (Emerald-Peridot-Rodingite-Nephrite jade) mineralization associated with ultramafic–mafic complexes of Pakistan. *Geol. Soc. Lond. Spec. Publ.* **2026**, *552*, 101–148. [CrossRef]
44. Obiadi, S.S.; Amini, M.A.; Fazli, F. Mineralogy and Geochemistry of Nephrite from Wolay Deposited, Kunar, East Afghanistan. *J. Mech. Civ. Ind. Eng.* **2020**, *3*, 56–65. [CrossRef]
45. Amin, U.; Zaheer, H.; Salih, A.H.; Bawary, A.F.; Noorzai, S.; Noori, U.; Nader, S. Understanding Chemical and Mineralogical Composition of Nahartangi Nephrite from Goshta. *J. Mech. Civ. Ind. Eng.* **2023**, *4*, 1–7. [CrossRef]
46. Pham, V.L.; Giuliani, G.; Garnier, V.; Ohnenstetter, D. Gemstones in Vietnam—A review. *Austral. Gem.* **2004**, *22*, 162–168.
47. Lindley, I.D.; White, P.J.S. A review of the occurrence of and potential for jade in the New Guinea Mobile Belt. *Austral. J. Earth Sci.* **2022**, *69*, 453–472. [CrossRef]
48. Boyd, W.F.; Wight, W. Gemstones of Canada. *J. Gemm.* **1983**, *18*, 544–562. [CrossRef]
49. Simandl, G.J.; Riveros, C.P.; Schiarizza, P. Nephrite (Jade) Deposits, Mount Ogden Area, Central British Columbia (NTS 093N 13W). In *Geological Fieldwork 1999*; British Columbia Geological Survey: Victoria, BC, Canada, 2000; pp. 339–347.
50. Jiang, B.; Bai, F.; Zhao, J. Mineralogical and geochemical characteristics of green nephrite from Kutcho, northern British Columbia, Canada. *Lithos* **2021**, *388*, 106030. [CrossRef]
51. Liu, K.; Wen, J.; Zhai, H.; Lu, K.; Shi, G. Berry-shaped, vivid green grossular within green nephrite from the Polar deposit, Canada. *Minerals* **2026**, *16*, 188. [CrossRef]
52. Jutras, J.-P.; Williams, C.; Williams, B.; Rossman, G.R. Nephrite Jade from Washington State, USA, Including a New Variety Showing Optical Phenomena. *J. Gemol.* **2023**, *38*, 494–511. [CrossRef]
53. Mustoe, G.E. Nephrite Jade and Related Rocks from Western Washington State, USA: A Geologic Overview. *Minerals* **2024**, *14*, 1186. [CrossRef]
54. Mustoe, G.E. Pleistocene Glacial Transport of Nephrite Jade from British Columbia, Canada, to Coastal Washington State, USA. *Geosciences* **2024**, *14*, 242. [CrossRef]
55. Mills, J. Nephrite with Magnetite Inclusions In San Bernardino County, California. *Rocks Miner.* **2021**, *96*, 442–448. [CrossRef]
56. Root, F.K. *Wyoming Jade: Information Circular*; The Geological Survey of Wyoming: Laramie, WY, USA, 1985; 8p.
57. Sutherland, W.M. *Gemstones, Lapidary Materials, and Geological Collectables in Wyoming: Open File Report 90-9*; The Geological Survey of Wyoming: Laramie, WY, USA, 1990; 53p. and 2 maps.
58. Dan Hausel, W.; Sutherland, W.M. *Gemstones and Other Unique Minerals and Rocks of Wyoming: A Field Guide for Collectors (Bulletin)*; Wyoming State Geological Survey: Laramie, WY, USA, 2000; Volume 71, 289p.
59. Dan Hausel, W. *Minerals and Rocks of Wyoming: A Guide for Collectors, Prospectors and Rock Haunds*; The Geological Survey of Wyoming: Laramie, WY, USA, 2005; 168p.
60. Gil, G.; Barnes, J.D.; Boschi, C.; Gunia, P.; Szakmany, G.; Bendo, Z.; Raczynski, P.; Peterdi, B. Origin of serpentinite-related nephrite from Jordanów and adjacent areas (SW Poland) and its comparison with selected nephrite occurrences. *Geol. Quart.* **2015**, *59*, 457–472. [CrossRef]
61. Jutras, J.-P.; Williams, C.; Williams, B.; Ream, L. Nephrite Jade from the Sky Zone, Wyoming, USA: Characteristics and Primary Hydrothermal Origin. *J. Gemol.* **2024**, *39*, 36–53. [CrossRef]
62. Lobos, K.; Sachanbinski, M.; Pawlik, T. Nephrite from Naslawice in Lower Silesia (SW Poland). *Prz. Geol.* **2008**, *56*, 991–999. (In Polish with English abstract)

63. Gil, G.; Baginski, B.; Gunia, P.; Madej, S.; Sachanbinski, M.; Jokubauskas, P.; Belka, Z. Comparative Fe and Sr isotope study of nephrite deposits hosted in dolomitic marbles and serpentinites from the Sudetes, SW Poland: Implications for Fe-As-Au-bearing skarn formation and post-obduction evolution of the oceanic lithosphere. *Ore Geol. Rev.* **2020**, *118*, 103335. [CrossRef]
64. Cooper, A.F. Nephrite and metagabbro in the Haast Schist at Muddy Creek, northwest Otago, New Zealand. *N. Z. J. Geol. Geophys.* **1995**, *38*, 325–332. [CrossRef]
65. Cooper, A.F. Origin and evolution of nephrites, diopsidites and giant diopside crystals from the contact zones of the Pounamu Ultramafics, Westland, New Zealand. *N. Z. J. Geol. Geophys.* **2023**, *66*, 88–101. [CrossRef]
66. Wilkins, C.J.; Tennant, W.C.; Williamson, B.E.; McCammon, C.A. Spectroscopic and related evidence on the coloring and constitution of New Zealand jade. *Am. Mineral.* **2003**, *88*, 1336–1344. [CrossRef]
67. Adams, C.J.; Beck, R.J.; Campbell, H.J. Characterisation and origin of New Zealand nephrite jade using its strontium isotopic signature. *Lithos* **2007**, *97*, 307–322. [CrossRef]
68. Grapes, R.H.; Yun, S.T. Geochemistry of a New Zealand nephrite weathering rind. *N. Z. J. Geol. Geophys.* **2010**, *53*, 413–426. [CrossRef]
69. Tarling, M.S.; Smith, S.A.F.; Negrini, M.; Kuo, L.-W.; Wu, W.-H.; Cooper, A.F. An evolutionary model and classification scheme for nephrite jade based on veining, fabric development, and the role of dissolution–precipitation. *Sci. Rep.* **2022**, *12*, 7823. [CrossRef] [PubMed]
70. Hockley, J.J. Nephrite (jade) Occurrence in the Great Serpentine Belt of New South Wales, Australia. *Nature* **1974**, *247*, 364. [CrossRef]
71. Coenraads, R.R. Gemstones of New South Wales. *Austral. Gem.* **1995**, *19*, 91–107.
72. Dobretsov, N.L.; Tatarinov, A.V. *Jadeite and Nephrite in Ophiolites (on the Example of the Western Sayan)*; Nauka Publ.: Novosibirsk, Russia, 1983; 125p. (In Russian)
73. Sharp, Z.D. A laser-based microanalytical method for the in situ determination of oxygen isotope ratios of silicates and oxides. *Geochim. Cosmochim. Acta* **1990**, *54*, 1353–1357. [CrossRef]
74. Puzhakov, B.A.; Savelyev, V.P.; Kuznetsov, N.S.; Shokh, V.D.; Shchulkin, E.P.; Shchulkina, N.E.; Zhdanov, A.V.; Dolgova, O.Y.; Tarelkina, E.A.; Orlov, M.V. *State Geological Map of the Russian Federation. Scale 1: 1,000,000 (Third Generation). The Ural Series. Sheet N-41—Chelyabinsk. An Explanatory Note*; VSEGEI Cartographic Factory: St. Petersburg, Russia, 2013; 415p. (In Russian)
75. Warr, L.N. IMA–CNMNC approved mineral symbols. *Min. Mag.* **2021**, *85*, 291–320. [CrossRef]
76. Murzin, V.V.; Varlamov, D.A. Mineralogy and geochemistry of chloritolites in the area of the Nepryakhinsky gold field (Southern Urals). *Mineralogy* **2020**, *6*, 3–15. (In Russian) [CrossRef]
77. Siqin, B.; Qian, R.; Zhou, S.J.; Gan, F.X.; Dong, M.; Hua, Y.F. Glow discharge mass spectrometry studies on nephrite minerals formed by different metallogenic mechanisms and geological environments. *Int. J. Mass Spectrom.* **2012**, *309*, 206–211. [CrossRef]
78. Liu, Y.; Deng, J.; Shi, G.; Yui, T.-F.; Zhang, G.; Maituohuti, A.; Yang, L.; Sun, X. Geochemistry and petrology of nephrite from Alamas, Xinjiang, NW China. *J. Asian Earth Sci.* **2011**, *42*, 440–451. [CrossRef]
79. Kostov, R.I.; Protochristov, C.; Stoyanov, C.; Csedreki, L.; Simon, A.; Szikszai, Z.; Uzonyi, I.; Gaydarska, B.; Chapman, J. Micro-PIXE geochemical fingerprinting of nephrite neolithic artifacts from Southwest Bulgaria. *Geoarchaeology* **2012**, *27*, 457–469. [CrossRef]
80. Faure, G.; Mensing, T.M. *Isotopes: Principles and Applications*, 3rd ed.; John Wiley & Sons: New York, NY, USA, 2005; 928p.
81. Burtseva, M.V.; Ripp, G.S.; Posokhov, V.F.; Murzintseva, A.E. Nephrites of Eastern Siberia: Geochemical features and problems of genesis. *Russ. Geol. Geophys.* **2015**, *56*, 402–410. [CrossRef]
82. Rampilova, M.V.; Ripp, G.S.; Rampilov, M.O.; Damdinov, B.B.; Damdinova, L.B.; Posokhov, V.F. Isotope-Geochemical Features of Apoultrabasic Metasomatites of the Sayan–Baikal Folded Area. *Russ. Geol. Geophys.* **2021**, *62*, 1021–1035. [CrossRef]
83. Schmitt, A.K.; Liu, M.C.; Kohl, I.E. Sensitive and rapid oxygen isotopic analysis of nephrite jade using largegeometry SIMS. *J. Anal. At. Spectrom.* **2019**, *34*, 561–569. [CrossRef]
84. Liu, X.-F.; Zhang, H.-Q.; Liu, Y.; Zhang, J.; Li, Z.-J.; Zhang, J.-H.; Zheng, F. Mineralogical characteristics and genesis of green nephrite from the world. *Rocks Miner. Anal.* **2018**, *37*, 479–489. (In Chinese with English abstract)
85. Yui, T.-F.; Kwon, S.-T. Origin of a Dolomite-Related Jade Deposit at Chuncheon, Korea. *Econ. Geol.* **2002**, *97*, 593–601. [CrossRef]
86. Petrov, V.I.; Shalaginov, A.E.; Punegov, B.N.; Gorlova, L.I.; Zabelkina, L.G.; Grigorova, T.B.; Nikolsky, V.Y.; Shalaginova, T.I.; Petrova, A.S.; Sereda, V.V. *State Geological Map of the Russian Federation. Scale 1:200,000. Second Edition. The South Ural series. Sheet N-41-VII. Explanatory Note*; MF VSEGEI: Moscow, Russia, 2015; 168p. (In Russian)
87. Moiseev, A.P.; Nikolaeva, M.E. *Natural Monuments of the Chelyabinsk Region*; South Ural Publishing House: Chelyabinsk, Russia, 1987; 256p. (In Russian)
88. Kislov, E.V. *Natural Monuments (on the Example of Western Transbaikalia)*; Publishing House of the BSC SB RAS: Ulan-Ude, Russia, 1999; 180p. (In Russian)

Disclaimer/Publisher's Note: The statements, opinions and data contained in all publications are solely those of the individual author(s) and contributor(s) and not of MDPI and/or the editor(s). MDPI and/or the editor(s) disclaim responsibility for any injury to people or property resulting from any ideas, methods, instructions or products referred to in the content.